J Therm Anal Calorim (2014) 115:495–501
DOI 10.1007/s10973-013-3290-1

Influence of the synthesis parameters on the thermal behavior of some ZnO–starch composites

Bogdan Jurca · Alina Tirsoaga · Adelina Ianculescu · Oana Carp

Received: 7 February 2013 / Accepted: 7 June 2013 / Published online: 30 June 2013

Abstract Ten ZnO–starch composites were synthesized using a simple precipitation methodology. The IR spectroscopy and XRD investigations reveal the presence of amorphous starch and crystalline ZnO. The obtained composites present a spherical morphology, 5–8 spheres being interconnected into aggregates. The thermal analysis demonstrates that starch decomposition and ZnO thermally induced nucleation and crystal growth depending on the synthesis parameters such as starch processing (dissolution or gelatinization), reaction temperature (80, 90, and 100 °C), reaction time (15 min or 6 h), and applied treatments (heating or ultrasound irradiation).

Keywords ZnO · Starch · Composites · Thermoreactivity

Introduction

ZnO represents one of the most motivating materials due to its combination of interesting properties [semiconducting, piezoelectric, pyroelectric, and (photo)catalytical] [1] and implicit extensive applications in electronics (photoelectronics, sensors, and optical devices) [2–5]. The dependence of the materials properties on their size, shape, and crystalline structure has promoted the development of different preparation methodologies [6–9]. Although ZnO is an inexpensive material, many of these techniques (such as vapor-phase one) are costly, too complex or too difficult to be used in large-scale industrial production systems. Solution-phase routes (including precipitation [10, 11], hydrolysis [12], pyrolysis [13], sol–gel reaction [14, 15], wet polymerization method [16], microemulsions growth [17, 18], hydrothermal [19, 20] and solvothermal [21] synthesis, microwave assisted processes [22], etc.) are attractive due to their low-growth temperature (usually <200 °C), low cost, high efficiency, and potential for scale up. In addition, solution-based approaches have been successfully used to control the size and shape of ZnO crystals through the use of different organic molecules [23–25] or block copolymers [26].

On the other hand, the green synthesis of materials becomes an imperative up-to-date objective of the materials science. Polysaccharides represent one of the most environmental friendly raw materials that can be used as ingredients in materials synthesis [27, 28]. Among them, starch has a special position due to its abundance, widely available (the second most abundant biopolymer after cellulose), inexpensive cost, and functional versatility.

The present paper presents the thermal behavior of some ZnO–starch composites obtained by a simple precipitation method in the absence or presence of ultrasound irradiation, using starch as a green additive of the synthesis. The performed thermal analysis has three objectives. The first represents an assessment of how the experimental synthetic parameters (time, temperature, starch pre-gelatinization treatment, and the application of an ultrasound treatment) may influence the ZnO–starch interactions and the availability to undergo thermally induced processes such as nucleation and crystal growth, the present paper being the

B. Jurca · A. Tirsoaga
Physical Chemistry Department, University of Bucharest, Bd. Elisabeta 4-12, 030018 Bucharest, Romania

A. Ianculescu
Politehnica University of Bucharest, Gh. Polizu Street no. 1-7, 011061 Bucharest, Romania

O. Carp (✉)
Ilie Murgulescu Institute of Physical Chemistry, Romanian Academy, Splaiul Independentei 202, 060021 Bucharest, Romania
e-mail: dr_oana_carp@yahoo.com; ocarp@icf.ro

first one that reports such an investigation. It also provides informations about the obtained composition of the composites and the temperature range in which starch can be removed (considering that for some applications such as photocatalytical ones, it presence is not desired).

Experimental

Materials and synthesis method

All chemicals (analytical grade) were used as received without any further purification: soluble oxidized corn starch [$(C_6H_{10}O_5)_n$, Carl Roth, Germany, (S)], zinc acetate dihydrate [$Zn(CH_3COO)_2{\cdot}2H_2O$, Reactivul, Romania, (ZA)] and ammonium hydroxide solution (NH_4OH 25 %, Chimopar, Romania). The synthesis of zinc oxide–starch composite was performed via a precipitation procedure that uses either pre-dissolved (D) or pre-gelatinized (G) starch and a subsequent thermal (T), or ultrasound treatment (U).

In a typical procedure, an amount of 0.0978 g starch was dissolved in 110 mL hot water under stirring. For gelatinization, a heating treatment of 1 h at 80 °C followed by 1 h at 90 °C was supplementary performed. To obtain a molar ratio S/ZA equal with 0.15, the cooled starch solutions were mixed with 50 mL zinc acetate solution (80 mM). Afterward, the pH of the solutions mixture was adjusted to 10.35 by adding dropwise an aqueous solution of NH_4OH (2.88 M). A heating treatment at 80, 90, and 100 °C for 6 h or an ultrasound irradiation carried out with a sonochemical bath (Bandelin Electronic—Sonorex RK 100H—Germany, 35 kHz) for 15 min or 6 h under continuous stirring of the mixture led to the formation of a white colloidal solution that was subsequently centrifuged. The isolated product is washed several times with distilled water to remove the unreacted compounds, and finally dried on P_4O_{10}. The samples denoting and their synthesis parameters are summarized in Table 1.

Characterization

The infrared spectra were recorded from KBr pellets on a FTIR Brucker Tensor V-37 spectrophotometer. The crystalline structure of the obtained products was characterized by X-ray diffraction measurements carried out at room temperature with a SHIMADZU XRD 6000 diffractometer, using Ni-filtered Cu Kα radiation ($\lambda = 1.5418$ Å) for 2θ ranging between 20° and 80°. The morphology of as-synthesized zinc oxide was analyzed by scanning electron microscopy (SEM) using a Quanta 3D FEG microscope. The thermal measurements were performed on a Q-1500 Paulik–Paulik–Erdey derivatograph, in static air, with a heating rate of 10 °C min^{-1} and a sample mass of ~70–90 mg.

Results and discussion

Characterization of ZnO–starch composites

The FTIR spectra of the isolated sample reveal not only the presence of starch and ZnO, but also of bonded water. Figure 1 presents the spectra of the composites obtained after heating (100 °C, D100T and G100T) and ultrasound treatments (D15U and G15U) using pre-dissolved or pre-gelatinized starch. Starch characteristic peaks are presented at ~2,930 cm^{-1} [$\nu_{(C-H)}$ associated with ring methane hydrogen atoms] [29], in 1,550–1,300 cm^{-1} region [$\delta_{(OCH)}$, $\delta_{(COH)}$, $\delta_{(CCH)}$], ~1,150 cm^{-1} [$\nu_{(C-O)}$ of the C–O–H group], at ~1,080 and ~1,020 cm^{-1} [$\nu_{(C-O)}$ vibration of the C–O–C group of starch at anhydroglucose ring] [29, 30]. ZnO formation is confirmed by the strong absorption band from ~490 cm^{-1} corresponding to the stretching vibration of Zn–O originated from ZnO [31], while the water presence by the broad strong absorption from ~3,440 cm^{-1} and the medium one centered at ~1,645 cm^{-1}. The absorbance ratio 1,080/1,020 cm^{-1} may be used to quantify the starch's order degree: a decrease in intensity of the band from 1,080 cm^{-1} and, respectively, an increase in intensity of the one from ~1,020 cm^{-1} characterized the transition from a native to a gelatinized starch (loss of ordered structures) [32–34]. If in native starch, the absorbances ratio 1,080/1,020 cm^{-1} is equal with 0.86, it decreases in all the obtained samples, the variation being strongly dependent on the used synthesis conditions. For the composites obtained under heating treatment, the starch pre-treatment does not influence significantly the absorbance ratio evolution: an increase of the reaction temperature leads to a slightly and gradually decrease of this ratio for both types of composites. In the case of an ultrasound irradiation, the starch gelatinization causes an abrupt and noticeable decrease of the absorbance ratio, effect that is not evidenced for starch's pre-dissolved samples. In the particular case presented in Fig. 1, the absorbance ratios 1,080/1,020 cm^{-1} are equal with 0.78/0.72 for D100T/G100T samples, and 0.75/0.54 for D15U/G15U ones.

The XRD pattern of the uncalcinated ZnO–starch composites is characteristic for ZnO wurtzite structure, no supplementary peak being registered, fact that demonstrates both the formation of ZnO during the synthesis procedure, and the presence in the as-prepared composites of amorphous starch (Fig. 2). As expected, the crystallinity degree of ZnO in the synthesized composites (evaluated considering a reference sample of commercial ZnO-Merck)

Table 1 Samples denoting, synthesis parameters, composition and structural characterization

Sample	Starch processing treatment	Synthesis parameters	Composition (molar ratio) ZnO:starch:H_2O[a]	Crystallinity/ %[b]
D80T	Dissolved	80 °C, 6 h	19:1:3	60
D90T	Dissolved	90 °C, 6 h	16:1:2	67
D100T	Dissolved	100 °C, 6 h	18:1:2	71
G80T	Gelatinized	80 °C, 6 h	17:1:3	64
G90T	Gelatinized	90 °C, 6 h	16:1:3	70
G100T	Gelatinized	100 °C, 6 h	19:1:3	78
D15U	Dissolved	Ultrasound, 15 min	16:1:3	73
G 15U	Gelatinized	Ultrasound, 15 min	13:1:3	77
D6U	Dissolved	Ultrasound, 6 h	18:1:3	80
G6U	Gelatinized	Ultrasound, 6 h	19:1:3	88

[a] Estimated from thermogravimetric results

[b] Evaluated considering a reference sample of ZnO-Merck

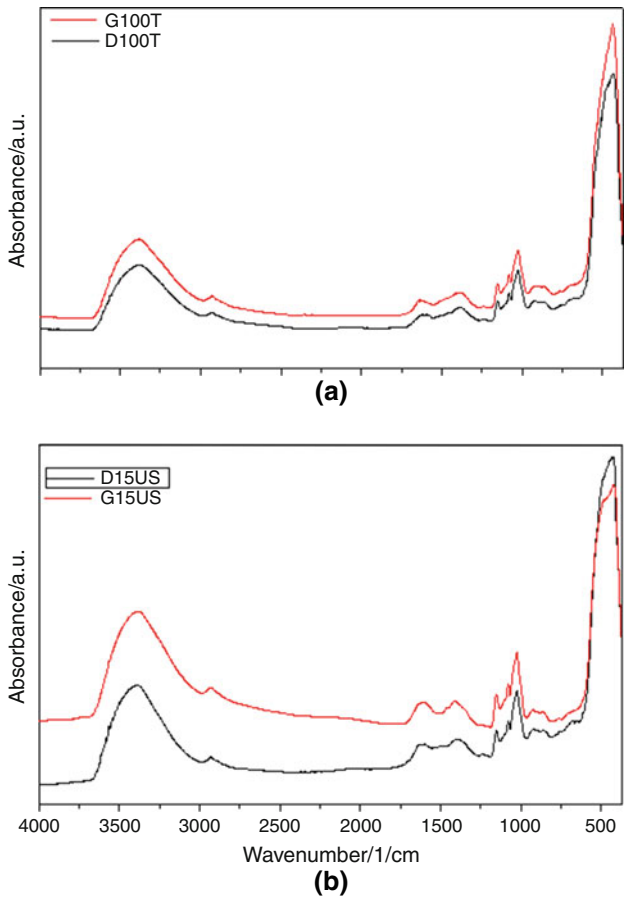

Fig. 1 FTIR spectra of ZnO–starch composite: **a** D100T and G100T, **b** D15US and G15US

increases with reaction temperature and time, being higher for the samples obtained with pre-gelatinized starch and for the ultrasound treated ones (Table 1).

The starch presence is critical in ZnO synthesis. First, it directs the reaction toward obtaining ZnO, in its absence the reaction products consist in a mixture of ZnO and $Zn(OH)_2$. Second, the long-chain biopolymer forces the nucleation and the initial growth of the crystallites to occur preferentially on polysaccharides backbone, inside regions of high concentrations of starch and Zn^{2+}, controlling the self-assembly of the 3-D architectures and leading to the formation of clusters of 5–8 spheres (aggregates sizes vary between ≈300 and 500 nm, Fig. 3). The shape and size of the aggregates are independent on synthesis parameters.

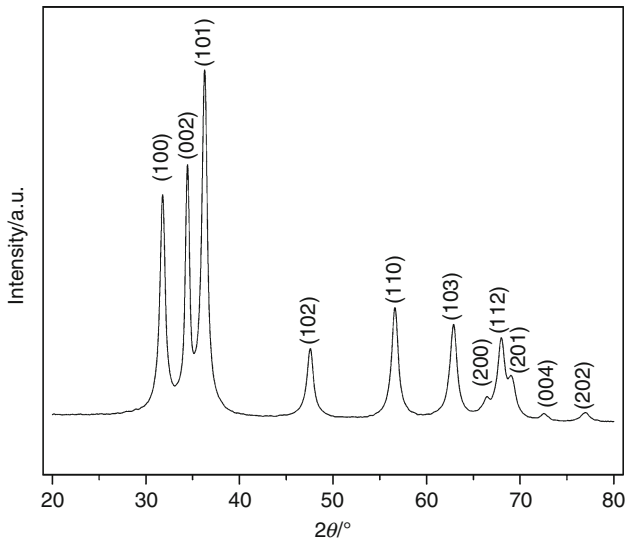

Fig. 2 XRD pattern of D80T ZnO–starch composite

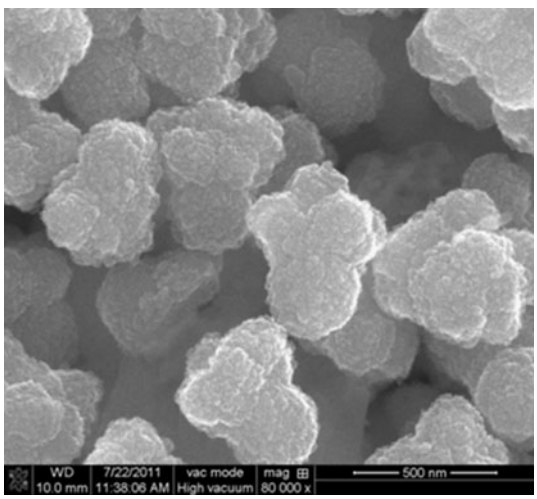

Fig. 3 SEM micrographs of G100T composite

Thermal decomposition of neat starch

Three decomposition steps are identified for starch decomposition (Fig. 4). The first mass loss [49.8–197.8 °C, mass loss (%) = 10.91) associated with an endothermic peak on the DTA curve corresponds to water elimination. The following two steps (227.1–602.5 °C) represent starch degradation. The first process (227.1–333.0 °C) starts as a non-oxidative breakdown of starch molecules coupled with an endothermic process that is converted at temperature rising to an exothermic one due to the combustion of the gaseous products. The second exothermic process is a glowing combustion (333–602.5 °C) during which the gasification of the carbonaceous residue formed in the previously degradation step takes place [35–38]. The initial endothermic effect is discriminated only at a heating rate of 10 °C min^{-1}, experimental condition that induces also a strong overlapping of the two combustion steps. Their separation becomes visible with the diminution of the heating rate (Fig. 5).

Thermal decomposition of ZnO–starch composites

The thermal degradation of the as-synthesized ZnO–starch samples occurs in several successive steps. Some of these are starch specific, others are related to ZnO presence.

All the investigated samples present similar mass losses stages: a dehydration one assigned to surface bonded water evolving that occurs in the temperature range ~50–170 °C followed by a two-stepped oxidative degradation of starch, degradation that takes place in the temperature interval ~175–500 °C. In the temperature interval ~470–690 °C several exothermic phase transitions occur, processes assigned to the crystallization and crystal growth of ZnO particles.

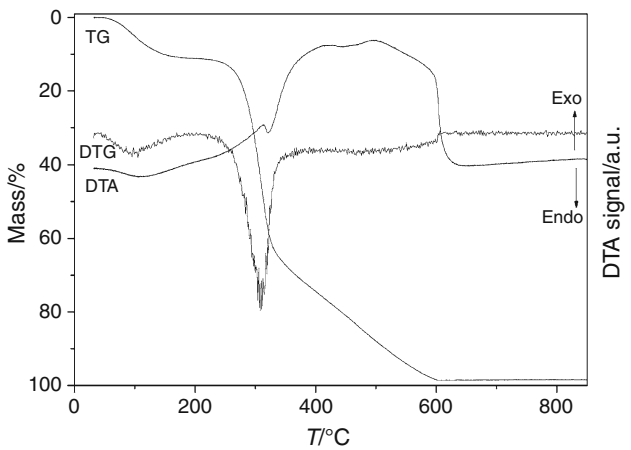

Fig. 4 Thermal curves (TG, DTG, and DTA) of neat starch

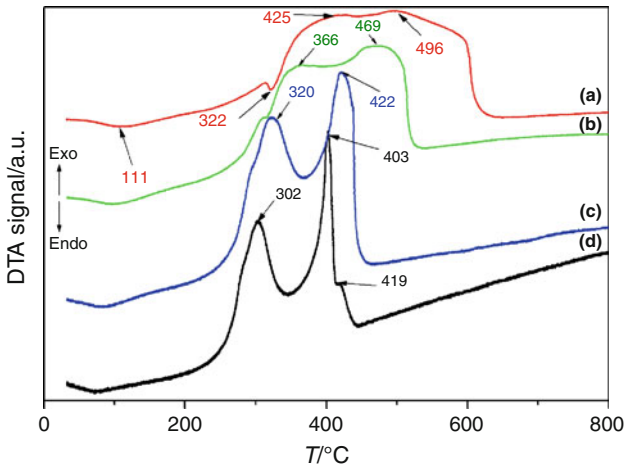

Fig. 5 DTA curves of neat starch at different heating rates: *a* 10 °C min^{-1}, *b* 5 °C min^{-1}, *c* 2.5 °C min^{-1}, and *d* 1.25 °C min^{-1}

The ZnO-linked starch thermochemistry is relatively different comparative with neat starch one in terms of temperature range of occurrence and magnitude. Thus, the temperature range of starch decomposition is with ~160 °C lower comparative with neat starch, the DTA maxima being with ~100 °C inferior than the one corresponding to unbounded starch (290–310 °C/390–410 °C for gaseous/glowing combustion) [35]. On the other hand, the second exothermic effect has a sensibly decreased magnitude. Such behavior is correlated to a catalytic effect of ZnO, that not only lower the degradation temperature but also accelerate the gasification of the carbonaceous residue, although the influence of starch transformations during the composites synthesis cannot be excluded (Fig. 6). None of the obtained DTA curves present the initial endothermic effect identified in starch degradation, although the used heating rate is the one at which such an effect was identified for pure starch.

From the obtained thermogravimetric data, a quantitative estimation of the molar compositions can be carried out (Table 1), the amount of polysaccharides included in Zn^{2+}-composites being the percent of mass loss registered for the second exothermic decomposition step. Since such an assessment can be made during the centrifugation stage of the synthesis, no sedimentation of soluble components is expected as oxidized starch does not retrograde [39], and consequently, the deposit obtained after centrifugation includes only insoluble forms of ZnO–polysaccharide composites.

The different amounts of starch contained by the composites can be understood as the result of two main processes: starch homogenization (including dissolution, gelatinization and/or solubilization phenomena) improved by higher temperature and longer heating treatment time, and the thermal stability of Zn^{2+}–starch complex (the stability constant is expected to decrease at higher temperature).

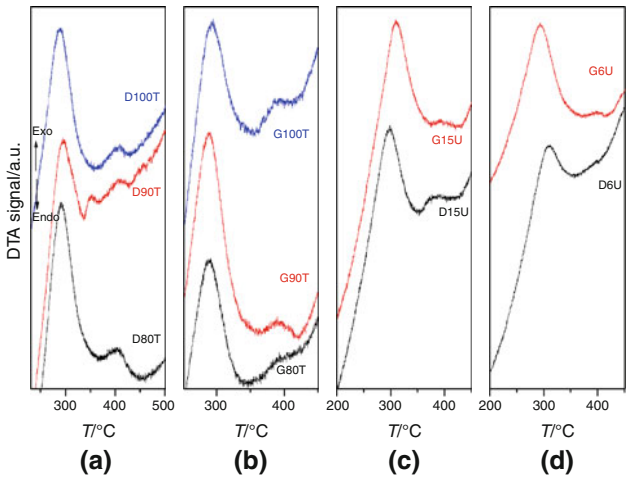

Fig. 6 DTA curves of starch degradation from ZnO–starch composites: **a** pre-dissolved starch and heating treatment (DT); **b** pre-gelatinized starch and heating treatment (GT); **c** pre-dissolved and pre-gelatinized starch and 15 min ultrasound treatment (D/G15U); and **d** pre-dissolved and pre-gelatinized starch and 6 h ultrasound treatment (D/G6U)

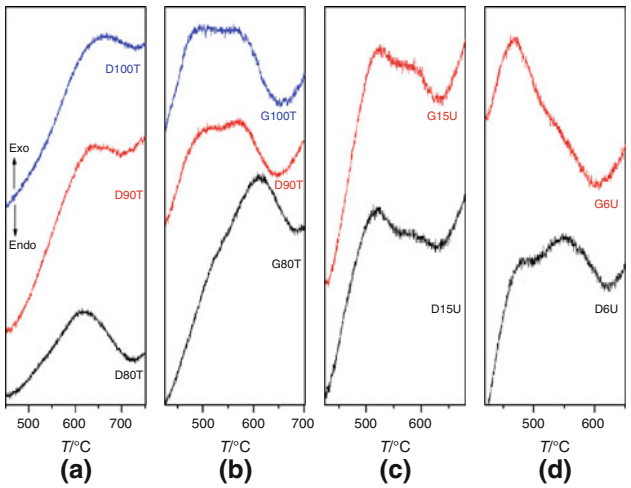

Fig. 7 DTA curves of nucleation/growth of ZnO from ZnO–starch composites: **a** pre-dissolved starch and heating treatment (DT); **b** pre-gelatinized starch and heating treatment (GT); **c** pre-dissolved and pre-gelatinized starch and 15 min ultrasound treatment (D/G15U); and **d** pre-dissolved and pre-gelatinized starch and 6 h ultrasound treatment (D/G6U)

In the series of composites obtained by the heating method, the samples prepared at 90 °C present the highest polysaccharide content [mass loss (%) = 10.57/10.49 for D90T/G90T]. Either a lower or a higher temperature during the synthesis leads to slightly lower values of the mass losses, behavior that has different reasons. If for the composites obtained at 100 °C an inferior stability of the Zn^{2+}–starch complex is expected, a lower synthesis temperature causes a different starch homogenization during the reaction with Zn^{2+} species.

Both the composites obtained under 15 min of ultrasound irradiation present high-polysaccharide content [mass loss (%) = 10.72/13.01 for D15U/G15U], the sample that used gelatinized starch being characterized by the highest starch concentration, meaning that an optimum of the synthesis parameters (mainly homogenization) is achieved regarding of Zn^{2+}-complex formation.

The samples obtained by a longer ultrasound irradiation time (6 h) contain a smaller amount of starch [mass loss (%) = 9.9/9.25 for D16U/G6U]. Such effects could be related with the break-down (depolymerization) of starch polymer determined by the longer time of energetic ultrasound treatment [40]. Gelatinized starch should be therefore stronger degraded than dissolved one [41], which may explain the smaller amount of the removed organic compound in the sample G6U compared to D6U.

The exothermic processes positioned above 460 °C are assigned to the nucleation and growth of the solid ZnO particles (Fig. 7). Previous studies on nanocrystalline ZnO powders [42] evidenced that nucleation and, respectively, growth exothermic effects are well separated when a high-heating rate (20 °C min^{-1}) is used, the corresponding DSC maxima being located at 465 and 500 °C. The heating rate decrease determines an increase of the overlapping of these two exothermic effects, together with a shift toward lower temperature values of the corresponding DSC peaks (i.e., for 10 °C min^{-1}: 430 and 465 °C, respectively). In the case of the investigated samples, the above-mentioned processes occur at higher temperatures than pure in ZnO due to the initial burning of the carbonaceous material.

The samples D80T, D90T, and D100T prepared with pre-dissolved starch solution present a relatively broad exothermic effect with a similar DTA shape and a maximum that follow the order: 615 °C (D80T) > 633 °C (D90T) > 660 °C (D100T) (Fig. 7a). This sequence can be related to the uniformity of zinc distribution along the polysaccharide chains: a better separation of the ZnO domains by the organic component induces a crystalline growth at higher temperatures after the removal of the carbonaceous residues. Because no distinct exothermic effect correlated with nucleation is observed, the overall process may be associated mainly with ZnO particles growth.

In the case of the samples prepared with pre-gelatinized starch solution, G80T, G90T, and G100T, the thermal behavior is not so unitary (Fig. 7b). The DTA signal of G80T is characterized by a single maximum at 612 °C, the curve profile being similar to D80T sample. For G90T and G100T samples, a broad plateau-shape exothermic region with not well-defined maxima starts at 512 and, respectively, 484 °C up to 572 °C. A plausible explanation of the

obtained profile is an overlapping in the investigated temperature range of the nucleation with growth processes. The increased homogenization of the gelatinized starch comparative to the dissolved one may determine a more uniform Zn^{2+}/polysaccharide distribution and as consequence, the exothermic effects are shifted at lower temperatures. For the G80T sample, the synthesis temperature (80 °C) seems to be too low for a proper homogenization, hence only minor differences are observed if pre-dissolved or pre-gelatinized starch is used.

The application of an ultrasound irradiation alters the influence of the different starch preheating treatments (dissolution vs. gelatinization). A short ultrasound irradiation time (15 min) generates a similar thermal behavior in the investigated interval (Fig. 7c): a broad DTA peak with a quasi-plateau between two DTA maxima, 522/519 °C (D15U/G15U) and 593/590 °C (D15U/G15U). The DTA signals (Figs. 6c, 7c) of the composites containing dissolved and gelatinized starch are similar, behaviour that may be explained by the similar Zn^{2+}/polysaccharide distribution induced by the ultrasound irradiation.

A longer ultrasound irradiation time (6 h) determines a shift of the two DTA maxima to lower temperature values (Fig. 7d), the shape of the DTA curves depending on the used starch pre-heating treatments. The sample D6U presents a better separation of the peaks, although a certain overlapping is also noticed: the first maximum registered at 480 °C may be attributed mainly to ZnO nucleation and the slightly more intense one from 550 °C can be caused by ZnO growth. The maxima temperatures of G6U are shifted to lower values: 470 °C as a relatively strong and well-defined exothermic effect, followed by a weak shoulder at 540 °C. Such behavior could be connected to a better crystallization of the ZnO during the prolonged ultrasound treatment, the XRD analysis confirming for this sample the best crystallization degree of the ZnO (Table 1).

Conclusions

The thermal behavior of the ZnO–starch composites consists of three decomposition stages, a dehydration assigned to water evolving (~50–170 °C) and a two-step starch degradation (175–500 °C), followed by phase transformation processes (~470–690 °C) assigned to the ZnO crystallization and crystal growth. The starch decomposition is different comparative with pure starch. The degradation occurs at lower temperature ranges, being associated with an inferior exothermic effect, behavior attributed to the catalytic effect of ZnO.

The registered starch content is explained as a result of two processes, starch homogenization in reaction medium, and Zn^{2+}–starch complex thermal stability. The samples submitted for 15 min to an ultrasound irradiation present the highest polysaccharide content because of an optimum synthesis in terms of Zn^{2+}-complex formation and the absence of polysaccharides chains breaking-down reactions.

The nucleation and crystal growth processes of ZnO that follow the burning of the carbonaceous materials occur at higher temperatures than in bulk oxide. The lowest temperatures are registered for the samples ultrasound irradiated for 6 h, due to a better ZnO crystallization during the synthesis.

Our present investigations confirm the applicability of the thermal analysis as a valuable tool for a quantitative and qualitative characterization of the organic–inorganic composites.

Acknowledgements The paper done within the research program: "Biophysical and green chemistry applications" of the "Ilie Murgulescu" Institute of Physical Chemistry of the Romanian Academy was supported by a grant of the Romanian National Authority for Scientific Research, CNCS-UEFISCDI, project number PN-II-ID-PCE-2011-3-0473.

References

1. Liqiang J, Yichun Q, Baiqi W, Shudan L, Baojiang J, Libin Y, Wei F, Honggang F, Jiazhong S. Review of photoluminescence performance of nano-sized semiconductor materials and its relationships with photocatalytic activity. Sol Energy Mater Sol Cells. 2006;90:1773–87.
2. Xia YN, Yang PD, Sun YG, Wu YY, Mayers B, Gates B, Yin YD, Kim F, Yan HQ. One-dimensional nanostructures: synthesis, characterization, and applications. Adv Mater. 2003;15:353–89.
3. Gao PX, Wang ZL. Mesoporous polyhedral cages and shells formed by textured self-assembly of ZnO nanocrystals. J Am Chem Soc. 2003;125:11299–305.
4. Wang XD, Summers CJ, Wang ZL. Large-scale hexagonal-patterned growth of aligned ZnO nanorods for nano-optoelectronics and nanosensor arrays. Nano Lett. 2004;4:423–6.
5. Shen GZ, Bando Y, Lee CJ. Synthesis and evolution of novel hollow ZnO urchins by a simple thermal evaporation process. J Phys Chem B. 2005;109:10578–83.
6. Ghoshal T, Kar S, Chaudhuri S. ZnO doughnuts: controlled synthesis, growth mechanism, and optical properties. Cryst Growth Des. 2007;7:136–41.
7. Wu QZ, Chen X, Zhang P, Han YC, Chen XM, Yan YH, Li SP. Amino acid-assisted synthesis of ZnO hierarchical architectures and their novel photocatalytic activities. Cryst Growth Des. 2008;8:3010–8.
8. Zhang J, Sun L, Yin J, Su H, Liao C, Yan C. Control of ZnO morphology via a simple solution route. Chem Mater. 2002;14:4172–7.
9. Jang ES, Won JH, Hwang SJ, Choy JH. Fine tuning of the face orientation of ZnO crystals to optimize their photocatalytic activity. Adv Mater. 2006;18:3309–12.
10. Cao MIY, Liu B, Huang R, Xia Z, Ge S. Flash synthesis of flower-like ZnO nanostructures by microwave-induced combustion process. Mater Lett. 2011;65:160–3.
11. Wang Y, Zhang C, Bi S, Luo G. Preparation of ZnO nanoparticles using the direct precipitation method in a membrane dispersion micro-structured reactor. Powder Technol. 2010;202:30–6.

12. Jezequel D, Guenot J, Jouini N, Fievet F. Submicrometer zinc oxide particles: elaboration in polyol medium and morphological characteristics. J Mater Res. 1995;10:77–83.
13. Milosevic O, Uskokovic D. Synthesis of $BaTiO_3$ and ZnO varistor precursor powders by reaction spray pyrolysis. Mater Sci Eng A. 1993;168:249–52.
14. Spanhel L. Colloidal ZnO nanostructures and functional coatings: a survey. J Sol–Gel Sci Technol. 2006;39:7–24.
15. Cheng HM, Hsu HC, Chen SL, Wu WT, Kao CC, Lin LJ, Hsieh WFJ. Efficient UV photoluminescence from monodispersed secondary ZnO colloidal spheres synthesized by sol–gel method. Cryst Growth. 2005;277:192–9.
16. Ying KL, Hsieh TE, Hsieh YF. Colloidal dispersion of nano-scale ZnO powders using amphibious and anionic polyelectrolytes. Ceram Int. 2009;35:1165–71.
17. Kaneko D, Shouji H, Kawai T, Kon-No K. Synthesis of ZnO particles by ammonia-catalyzed hydrolysis of zinc dibutoxide in nonionic reversed micelles. Langmuir. 2000;16:4086–9.
18. Li X, HeG XiaoG, Liu H, Wang M. Synthesis and morphology control of ZnO nanostructures in microemulsions. J Colloid Interface Sci. 2009;333:465–73.
19. Liu B, Zeng HC. Hydrothermal synthesis of ZnO nanorods in the diameter regime of 50 nm. J Am Chem Soc. 2003;125: 4430–1.
20. Du GH, Xu F, Yuan ZY, Van Tendeloo G. Flowerlike ZnO nanocones and nanowires: preparation, structure, and luminescence. Appl Phys Lett. 2006;88:243101.
21. Ma J, Jiang C, Xiong Y, Xu G. Solvent-induced growth of ZnO microcrystals. Powder Technol. 2006;167:49–53.
22. Cho S, Jung SH, Lee KH. Morphology-controlled growth of ZnO nanostructures using microwave irradiation: from basic to complex structures. J Phys Chem C. 2008;112:12769–76.
23. Bauermann LP, del Campo A, Bill J, Aldinger F. Heterogeneous nucleation of ZnO using gelatin as the organic matrix. Chem Mater. 2006;18:2016–20.
24. Liu B, Zeng HC. Room temperature solution synthesis of monodispersed single-crystalline ZnO nanorods and derived hierarchical nanostructures. Langmuir. 2004;20:4196.
25. Kim C, Kim YJ, Jang ES, Yi GC, Kim HH. Whispering-gallery-modelike-enhanced emission from ZnO nanodisk. Appl Phys Lett. 2006;88:093104.
26. Taubert A, Palms D, Weiss O, Piccini MT, Batchelder DN. Polymer-assisted control of particle morphology and particle size of zinc oxide precipitated from aqueous solution. Chem Mater. 2002;14:2594–601.
27. Visinescu D, Patrinoiu G, Tirsoaga A, Carp O. Polysaccharides route: a new green strategy for oxides synthesis. In: Schwarbauer J, Lichtfouse E, editors. Environmentally chemistry for a sustainable world. Dordrecht: Springer; 2012. p. 119–69.
28. Nistor MT, Vasile C. Influence of the nanoparticle type on the thermal decomposition of the green starch/poly(vinyl alcohol)/montmorillonite nanocomposites. J Therm Anal Calorim. 2013; 111:1903–19.
29. Fang JM, Fowler PA, Tomkinson J, Hill CAS. The preparation and characterization of a series of chemically modified potato starches. Carbohydr Polym. 2002;47:245–52.
30. Ma XF, Yu JG, He K, Wang N. The effects of different plasticizers on the properties of thermoplastic starch as solid polymer electrolytes. Macromol Mater Eng. 2007;292:503–10.
31. Nakamoto K. Infrared and Raman spectra of inorganic and coordination compounds. 4th ed. New York: Wiley; 1986.
32. Van Soest JJG, Tournois H, de Wit D, Vliegenthart JFG. Short-range structure in (partially) crystalline potato starch determined with attenuated total reflectance Fourier-transform IR spectroscopy. Carbohydr Res. 1995;279:201–14.
33. Rubens P, Snauwaert J, Heremans K, Stute R. In situ observation of pressure-induced gelation of starches studied with FTIR in the diamond anvil cell. Carbohydr Polym. 1999;39:231.
34. Sevenou O, Hill SE, Farhat IA, Mitchell JR. Organization of the external region of the starch granule as determined by infrared microscopy. Int J Biol Macromol. 2002;31:79–85.
35. Aggarwal K, Dollimore D, Heaon K. Comparative thermal analysis of two biopolymers, starch and cellulose. J Therm Anal. 1997;50:7–17.
36. Beninca C, Colman TAD, Lacerda LG, da Silva Carvalho Filho MA, Demiate IM, Bannach G, Schnitzler E. Thermal, rheological, and structural behaviors of natural and modified cassava starch granules, with sodium hypochlorite solutions. J Therm Anal Calorim. 2013;111:2217–22.
37. Horváth E. Thermal analysis of starch for realizing embedded channel in low temperature co-fired ceramic. J Therm Anal Calorim. 2013. doi 10.1007/s10973-012-2877-2.
38. Colman TAD, Demiate IM, Schnitzler E. The effect of microwave radiation on some thermal, rheological and structural properties of cassava starch. J Therm Anal Calorim. 2013. doi: 10.1007/s10973-012-2866-5.
39. Belitz HD, Grosch W, Schieberle P. Food chemistry. 4th ed. Berlin: Springer; 2009.
40. Sujka M, Jamroz J. Ultrasound-treated starch: SEM and TEM imaging, and functional behavior. Food Hydrocolloids. 2013;31: 413–9.
41. Iida Y, Tuziuti T, Yasui K, Towata A, Kozuka T. Control of viscosity in starch and polysaccharide solutions with ultrasound after gelatinization. Innov Food Sci Emerg Technol. 2008;9:140–6.
42. Marinkivic ZV, Mancic L, Milosevic O. The nature of structural changes in nanocrystalline ZnO powders under linear heating conditions. J Eur Ceram Soc. 2004;24:1929–33.